

# Electronic Visual Prosthesis

\*†Wentai Liu, †Mohanasankar Sivaprakasam, †Praveen R. Singh, †Rizwan Bashirullah,  
and \*†Guoxing Wang

\*Department of Electrical Engineering, University of California at Santa Cruz, CA; and †ECE Department, North Carolina State University, Raleigh, NC, USA

---

**Abstract:** Retinitis pigmentosa (RP) and age-related macular degeneration (AMD) are incurable diseases that result in profound vision loss due to degeneration of the light sensing photoreceptors. However, the discovery that direct electrical stimulation of the retinal neurons creates visual sensation has inspired prosthetic devices aimed to restore useful vision in RP/AMD patients. The approach to one such electronic visual prosthesis is described in this article. The prosthesis consists of an external unit and an internal unit. The communication link has three components—power and data transfer from the external to the internal unit, and data transfer from the internal to the external unit. A novel method of integrating power transfer and

back telemetry is described here. The goal is to design a stimulator chip with a small area with low power consumption. This chip, capable of stimulating 60 dedicated electrodes, is fabricated using AMI 1.2  $\mu\text{m}$  process technology and the results are presented. Improvements in the design to increase the number of outputs to 1,000 have been discussed. The new circuit is aimed at increasing the circuit density, reducing power per stimulus, and meeting the requirements more closely than the previous designs. The results of the designed chip are presented. **Key Words:** Retinal prosthesis—Telemetry—Neurostimulator—Inductive link—Low power design.

---

## INTRODUCTION

The possibilities of artificial vision by electrical stimulation are being investigated by many groups (1–5). While many approaches have been adopted, our group has focused on a epiretinal approach. Engineers of the Retinal Prosthesis Group at the University of California at Santa Cruz, along with medical researchers at the University of Southern California and our other research partners, have developed several generations of stimulation integrated circuits (ICs) (Fig. 1). These ICs are designed to deliver current pulses for retinal stimulation, as determined by clinical studies conducted on the visually impaired with retinitis pigmentosa (RP) and age-related macular degeneration (AMD) (6). Our first chip, Retina-1, had a  $5 \times 5$  photo sensor array and current drivers and was fabricated using 2.0  $\mu\text{m}$  technology. Based on studies of this chip, it was con-

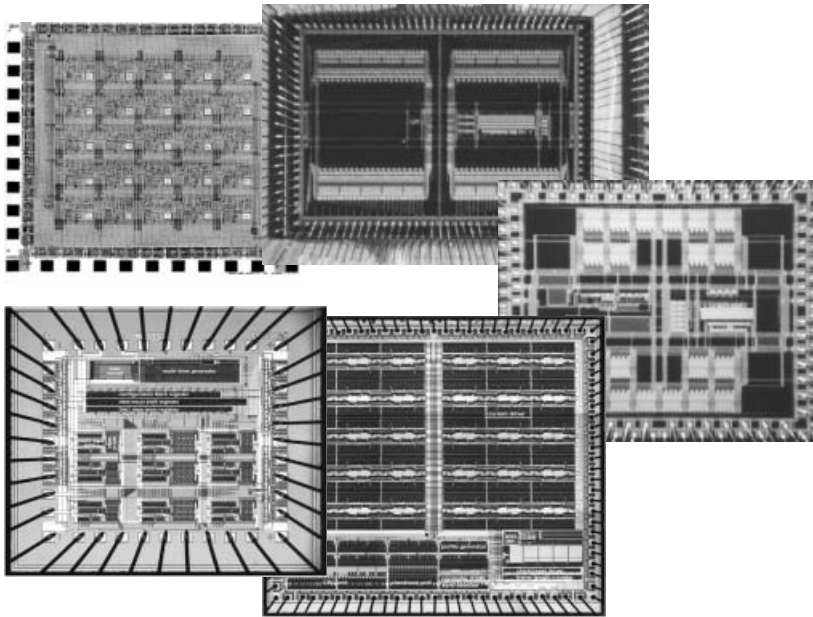
cluded that the photo sensor array on the implanted chip is not a viable solution. First, variation in the intensity of light makes the design complex, increasing the chip size. Second, the large power requirement for such sensing circuits is hard to meet. So, the photo sensing circuits were shifted outside the eye and data link was established. The Retina-2 chip had 100 channels, with 20 drivers and  $1 \times 5$  multiplexing. It also had 200, 400, and 600  $\mu\text{A}$  full scale current scalability. It had single rail supply voltage and a single current source with a bridge circuit providing both cathodic and anodic currents. This chip was also fabricated using 2.0  $\mu\text{m}$  technology. The Retina-3 chip had additional circuitry for data recovery from a data link. An amplitude shift keying (ASK) demodulator and delay locked loop (DLL) were used for alternate pulse width modulation (PWM) data recovery. This chip was fabricated using AMI 1.2  $\mu\text{m}$  technology.

The Retina-3.5/3.55 chips had 60 dedicated drivers and two independently programmable digital-to-analog converters (DACs) to provide more flexibility in the current waveform. The communication was strengthened through error detection using cyclic redundancy check (CRC) and checksum. This chip is

---

Received July 2003.

Address correspondence and reprint requests to Dr. Wentai Liu, Department of Electrical Engineering, University of California at Santa Cruz, 1156 High Street, Santa Cruz, CA 95064-1077, USA. E-mail: wentai@soe.ucsc.edu



Retinal chip	Salient features
Retina-1	5 × 5 Photo sensor array and current drivers; 2.0 μm CMOS technology
Retina-2	Photo sensors at the external side of the eye; 100 channels with 20 drivers (1 : 5 multiplexing); 2.0 μm CMOS technology
Retina-3	Additional circuitry for data recovery from PWM data link using ASK demodulator and DLL: AMI 1.2 μm technology
Retina-3.5/3.55	60 dedicated drivers; 2 independently programmable binary weighted DACs; error detection through CRC and check sum
Retina-4	Reduction of area using multibias DAC replacing the binary weighted DAC

FIG. 1. Evolution of the chips, Retina-1/2/3/3.55/4 (clockwise from top left).

discussed in detail in the next section. Because a binary weighted DAC increases the size of the most significant bit (MSB) devices by a factor of two for every bit of resolution, a smaller area multibias DAC was designed and tested in Retina-4 (7). This 8-bit multibias DAC reduces the DAC area by almost half. Other than ICs, a prototype image acquisition system using a miniature CMOS camera and an image processing system using a VLSI (very large-scale integration) image processing board has been built. Wireless communication electronics using a radio frequency link has been developed. The overall system, as shown in Fig. 2, consists of an external signal processing unit for CMOS camera output, a bi-directional

telemetry unit, an internal signal processing unit, a stimulus generator/driver, and an electrode array for interfacing to the retina.

## MATERIALS AND METHODS

### Telemetry

Previously, invasive tethering to implanted electronics using percutaneous connectors had been used to facilitate the studies of long-term biocompatibility and the investigation of the necessary signal pre-processing needed to enhance the performance of implants (8). However, percutaneous connectors increase the risk of infections as they cause a perpet-

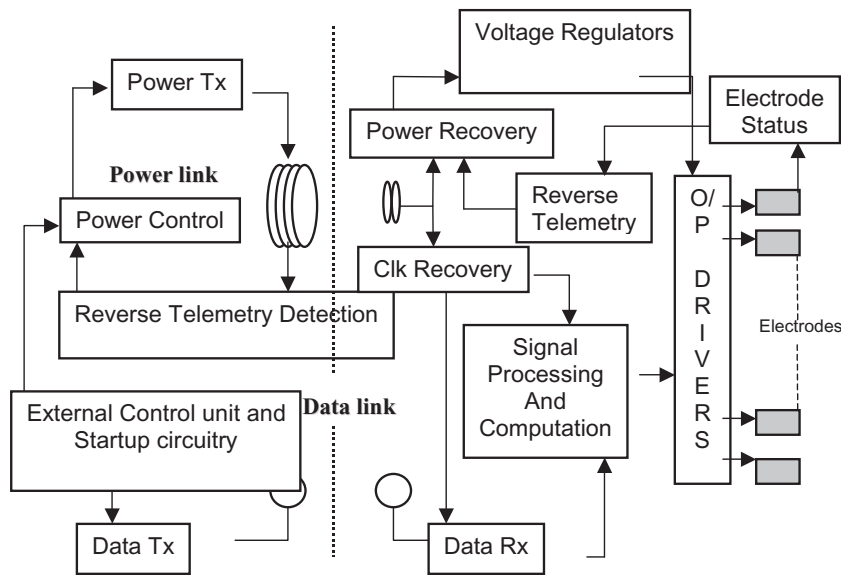


FIG. 2. Block diagram of the prosthesis. Tx, transmitter; Clk, clock; Rx, receiver; O/P, output.

ual breach of the body, require mechanical anchoring, and restrict eye movement. Moreover, due to high stimulus power requirement and small eye size, an implanted power source is not an option.

A number of advantages can be derived from partitioning the prosthesis into parts that are internal and external to the body, beyond merely simplifying the implantable unit. Primary benefits of external electronics include the decreased risk of adverse reaction to implanted materials, lower internal heat dissipation, and ease of refinement and upgrade of signal processing algorithms and functionality in the external components.

A wireless link is a viable approach to support the required data bandwidth and for providing adequate power to an implanted prosthesis. Furthermore, for the implant to monitor its device status, or perform self-diagnostics, there is also a need to transmit data to external devices. This functionality is termed as back telemetry. Therefore, in general, the long-term success of prostheses requires a telemetry link, which can provide adequate power to all implanted electronics and support a means to communicate information bi-directionally.

### Inductive telemetry

Magnetically coupled coils have been the standard means of wireless connection to implanted devices (9,10). Although there are many ways to transmit data to the implant, it has been the primary way to transfer a significant amount of power to the implant. Because the magnetic field strength over the coil axis falls as a third power of distance, this type of link is suitable only for very small distances. The primary

coil radiates energy widely in many directions. This is primarily the case when the magnetic field may not be directed due to the absence of magnetic material. The use of magnetic material should be avoided as it may lead to adverse effects if the individual were to come under the influence of an unwanted magnetic field. The radiation also imparts electromagnetic interference (EMI) to other nearby electrical devices and so care must be taken to meet the regulatory guidelines. Due to discontinuity at the body surface and the absence of magnetic material, for reasons explained above, the coils are air-coupled. Depending on the space between coils, air-coupling may result in very poor coupling coefficient between the coils.

Several studies have been conducted to measure the mutual inductance between two air-coupled coils (11–13). Coupling strength is dependent on coil loading, excitation frequency, coaxial alignment, coil separation, coil geometry, and angular alignment. Most of these are subject to variation in prostheses. Typical values for coil-coupling are between 0.01 and 0.1. To receive the required power at low coupling, high field strengths are used. Because the low frequency at which the coils operate does not have much of absorption in the tissue, this can be used safely. To achieve the required field strength with the small direct current (DC) supply, resonance is used. Resonance is achieved by placing an appropriate capacitor in parallel with the coil (14,15).

A back telemetry link for reverse data communication is used to transmit data from the implant to the external unit. These back telemetry data carry information on the status of the implant such as temperature, pH, power level, electrode impedance, and

other parameters reflecting the status of the implant, which will be of use in neural-recording, bio-function monitoring, and performing self-diagnostics. The efficiency of the power link is not affected much as the back telemetry link has a much lower data rate (few kbps) compared to the power link.

### Smart bi-directional inductive telemetry system for power and back telemetry

A class E driver is used as the power transmitter owing to its high efficiency and ability to generate a high field strength with low voltage power supply (16,17). The secondary coil is coupled with this field and resonated with an appropriate capacitor value at the operational frequency. The voltage regulators generate a dual rail supply of  $\pm 7$  V for the electrode stimulators and a 3-V supply for the digital logic. An initial shunt-type regulator provides current regulation and coarse voltage regulation. A series-type regulator provides the necessary fine voltage regulation required for subsequent stages.

The analog front-end also includes the passive back-telemetry unit for reverse data communication. Back telemetry is based upon the change in reflected impedance by the secondary on the primary. A change in the secondary impedance is achieved by

placing a MOS switch in series with the secondary coil. By this switch binary ASK data are imposed on the power carrier. Data detection on the primary side is accomplished by sensing the primary current in an inductor and by low pass filtering the analog waveform. Due to the relatively low frequency of the data compared to the power link frequency, power efficiency is not sacrificed.

It is recognized that the externally mounted primary coil is susceptible to changes in position and orientation. This variation may lead to a large variation in the mutual coefficient. In order to deliver a constant voltage to the load while accommodating this variation, large power dissipation is required in the regulation circuit. The problem is tackled by changing the system to a closed-loop one (Fig. 3). The secondary voltage is detected and the information is sent to the primary side through back telemetry (18). This information is used to adjust the primary excitation level to an optimal point of operation.

### Inductive data link

Two different methods of transmitting data from the external unit to the internal unit are described below. The first method employs ASK combined with

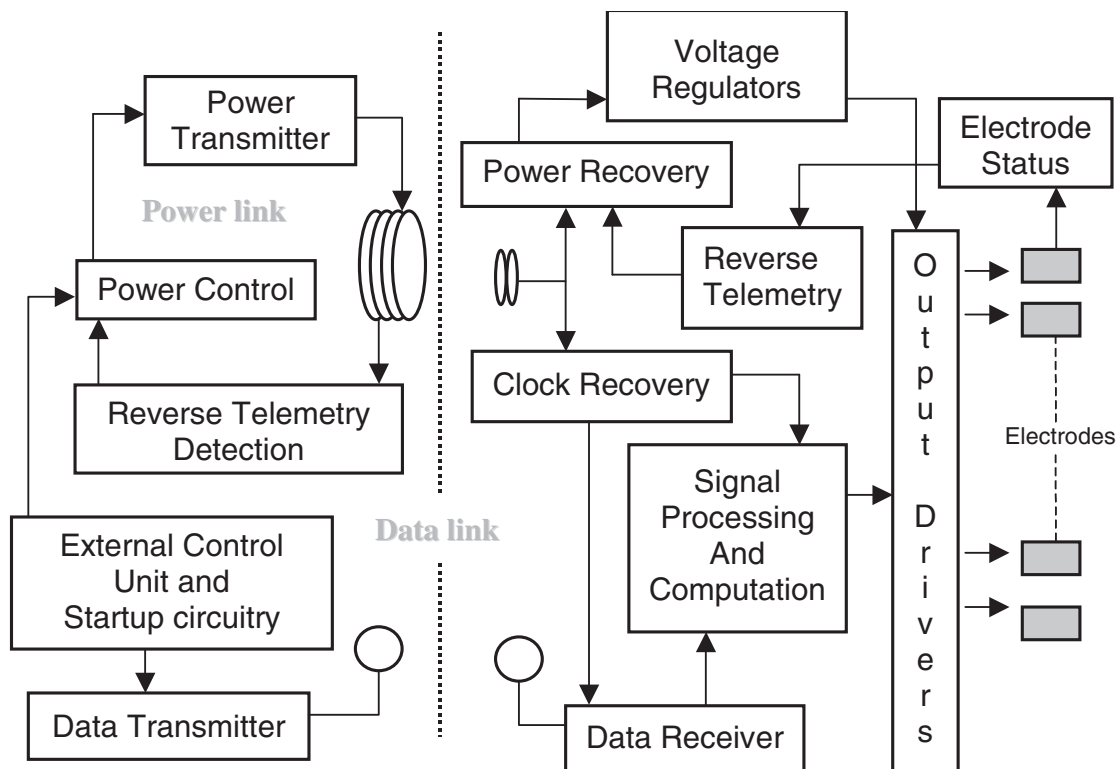


FIG. 3. System architecture of the smart bi-directional telemetry unit. RFC, radio frequency choke.

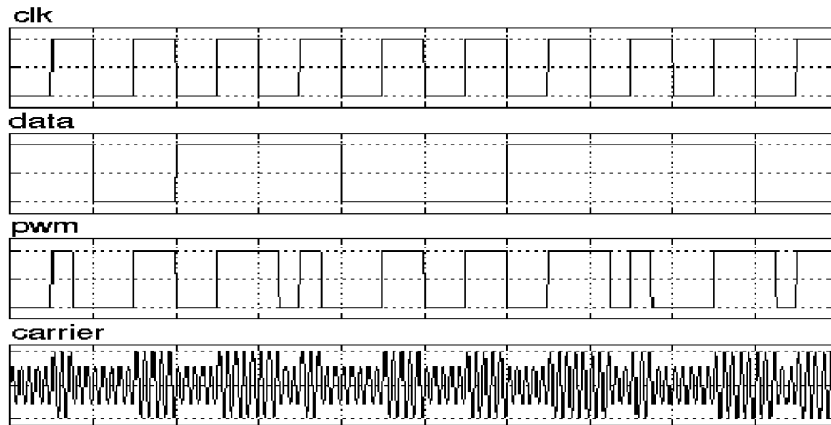


FIG. 4. Data link waveforms for PWM over ASK. clk, clock.

PWM modulation. This method sends data through the power carrier and operates at data rates from 25 to 250 kbps. The second method of data communication separates the inductive data link from the power link thereby achieving higher data rates.

#### Data link through PWM over ASK (25–250 kbps)

The waveforms related to this method of data transfer are shown in Fig. 4. ASK is used in order to reduce the circuit complexity and power consumption compared to the frequency modulation scheme. PWM is preferred over ASK because there is a possibility of misalignment in the external coil due to which the coupling coefficient may vary. Coupling variations by themselves will lead to signal amplitude variations and will be difficult to distinguish from the amplitude modulation. An alternative PWM scheme is used to obtain a zero DC signal. As a 10% modulation coefficient was chosen, a zero is encoded as a 50% duty cycle pulse, and ones are alternately encoded by 40 or 60% duty cycle pulses. This modulation method also eliminates the need of a local clock at the receiver. The rising edges of the PWM signal from the demodulator are fixed in time periodically and serve as a reference in the derivation of a clock signal. The data are encoded by the position of the falling transition at each pulse. The system is designed for PWM data ranging from 25 to 250 kbps with a carrier frequency ranging from 1 to 10 MHz.

At the receiver, the carrier envelope is passed to the ASK demodulator circuit to extract the digital (rail-to-rail) PWM waveform. The clock and data recovery circuit consists of a DLL and decoder logic. The DLL consists of a phase–frequency detector (PFD), a charge-pump, a loop filter, and a voltage-controlled delay line. The 36-stage delay line is locked to one period of the PWM waveform. The waveform is decoded by an XNOR gate whose inputs are the tapped-out signals at the 15th and the 21st

stages corresponding to the duty cycle percentages used in the PWM waveform. It is noticed that not only is a high data rate design difficult, but also a low data rate design. A challenge for the DLL design was to make the lockable frequency as low as 25 kHz without consuming a large chip area.

#### Dual band telemetry through differential binary phase shift keying (DBPSK; 1–2 Mbps)

The waveforms related to this method of data transfer are shown in Fig. 5. Current technologies for the telemetry between external and internal units in implantable systems are generally based on low frequency inductive links, because at low frequencies the human body is more penetrable to the magnetic field leading to higher efficiency wireless power transfer. While suitable for low data rate applications, this approach has the inherent limitation associated with Q-factor that causes a narrow band width. For 1,000 electrode outputs, stimulated at 60 Hz with approximately 20 bits per stimulus, the data rate needed will be 1.5–2 Mbps.

This approach achieves higher data rates by separating the data transmission from the power delivery, by allocating different frequencies for the power and forward telemetry data carriers. DBPSK modulation is used for its better signal-to-noise ratio with lesser complexity compared to other modulation techniques and its flexibility to use a noncoherent clock. The carrier frequency is 16 MHz. The nonreturn to zero (NRZ) data are encoded into the DBPSK signal through digital circuitry, modulated with the carrier frequency. The receiver has an amplifier, a high-pass filter to filter out the power interference, a demodulator, and a decoder to receive the transmitted data.

#### Architecture of the Retina-3.55 microstimulator

Recently developed, the Retina-3.55 IC is 4.6 mm × 4.7 mm in size and can stimulate 60 elec-

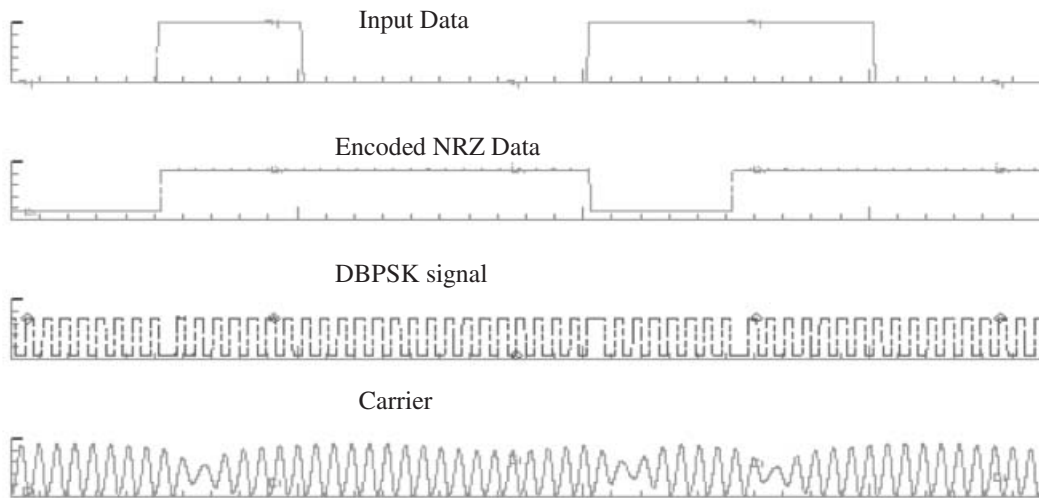


FIG. 5. Data link waveforms for the dual band telemetry. DBPSK, differential binary phase shift keying.

trodes with a safe and effective charge. Functional specifications for the IC operation require excitation currents up to 600  $\mu\text{A}$  amplitude, anodic and cathodic, delivered to retinal tissue with characterized impedance of approximately 10 k $\Omega$  (19). This requires a voltage drop of ( $\pm 6\text{ V}$  at the load and hence a ( $\pm 7\text{ V}$  power supply is required. Stimulation rates of at least 50 Hz are required for flicker-free vision. Required pulse widths and interphase delays are of the order of 1–5 ms. Charge-balanced pulses are a must for long-time compatibility in the biolog-

ical environment (see Fig. 6). The 60 current driver circuits are independently programmable.

**Retina-3.55 circuits**

The digital circuit primarily consists of data input, error detection, profile generation, data distribution to analog circuits and the control logic circuits. The communication protocol is implemented to operate in packet format each consisting of 1,024 bits. Each packet starts with a 16-bit synchronization word. The configuration packet sets the global parameters of

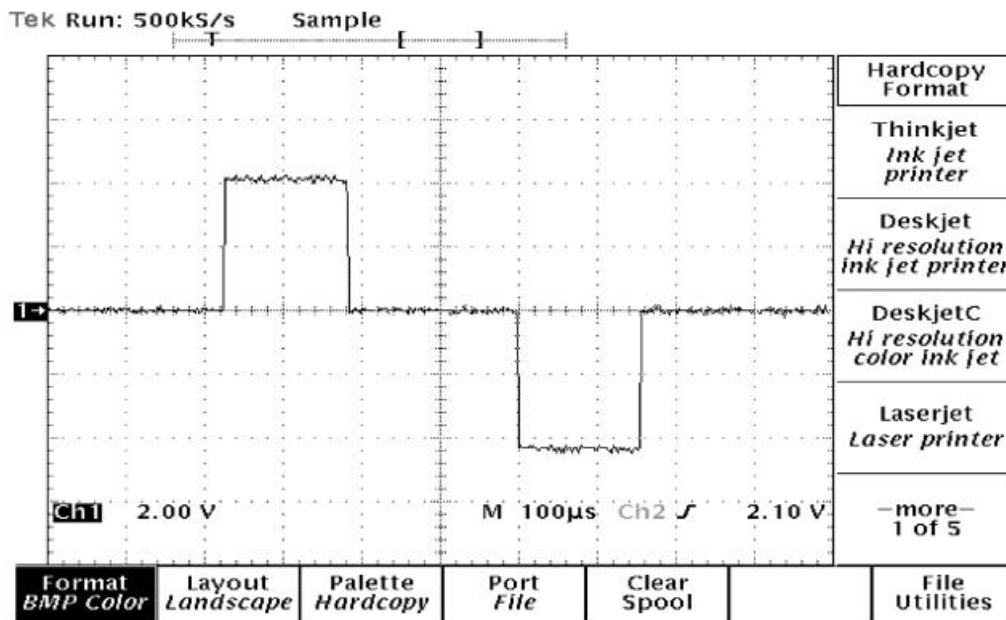


FIG. 6. Biphasic charge-balanced stimulation output.

the chip, such as timing for generating the pulse timing including the interphase delay, and current scaling factor. The data packet has information regarding the selection of appropriate timing profiles and the current amplitudes of anodic and cathodic outputs. The amplitude resolution is 4 bits. The pulse profile is generated through eight global, independently programmable pulse-timing references. The circuit works by comparing the start and stop time, given by the configuration packet, with a counter. An output waveform can be selected by choosing any two pairs, that is, one for anodic and one for cathodic provided they do not overlap. The communication of the data over the telemetry link will have a finite bit error rate (BER). Thus the data may have unintended consequences. To alleviate such problems every information packet has a 32-bit CRC as well as 16-bit checksum error. If an error is detected in the data packet the packet is not used. If an error is detected in the configuration frame, both the frame and the subsequent data packet are not used until a correct configuration packet is received (20).

Each of the 60 current drivers is capable of producing biphasic stimulus current using information provided in 16-bit data subpacket. The anodic current is sourced to the load by an ideal current source referenced to a positive supply of  $V_{dd}$  (see Fig. 7). Similarly, the cathodic current is sunk from the load

by an ideal current source referenced to a negative supply of  $V_{ss}$ . The driver employs two N-type metal-oxide-silicon field effect transistor (NMOS) binary-weighted current-mode DACs to produce the anodic and cathodic currents. The DAC currents are mirrored and scaled into an output circuit of high-voltage compliance. Each current driver contains two 8-to-1 multiplexers associated with DACs for programmable selection of any of the eight pulse timing profiles. One component of the driver circuit is a charge cancellation mechanism, which is intended to limit any unintentional accumulation of charge on the electrode. By periodically discharging the electrode outputs, the charge accumulated by mismatch and other process variations is removed. Using 2 bits from the configuration packet, the DAC biasing section can be tuned to mirror the bootstrap reference, which permits the global full-scale current output in the driver's biphasic amplifiers to be programmed at 200  $\mu\text{A}$ , 400  $\mu\text{A}$ , or 600  $\mu\text{A}$ .

#### Chip design for next generation retinal ICs

Recent studies suggest that a  $32 \times 32$  stimulus matrix will be required for face recognition (21). So our current work focuses on increasing the number of stimulating pixels in the retina from 60 to 1,000. It was concluded that by merely increasing the number of output channels in our present generation ICs, area

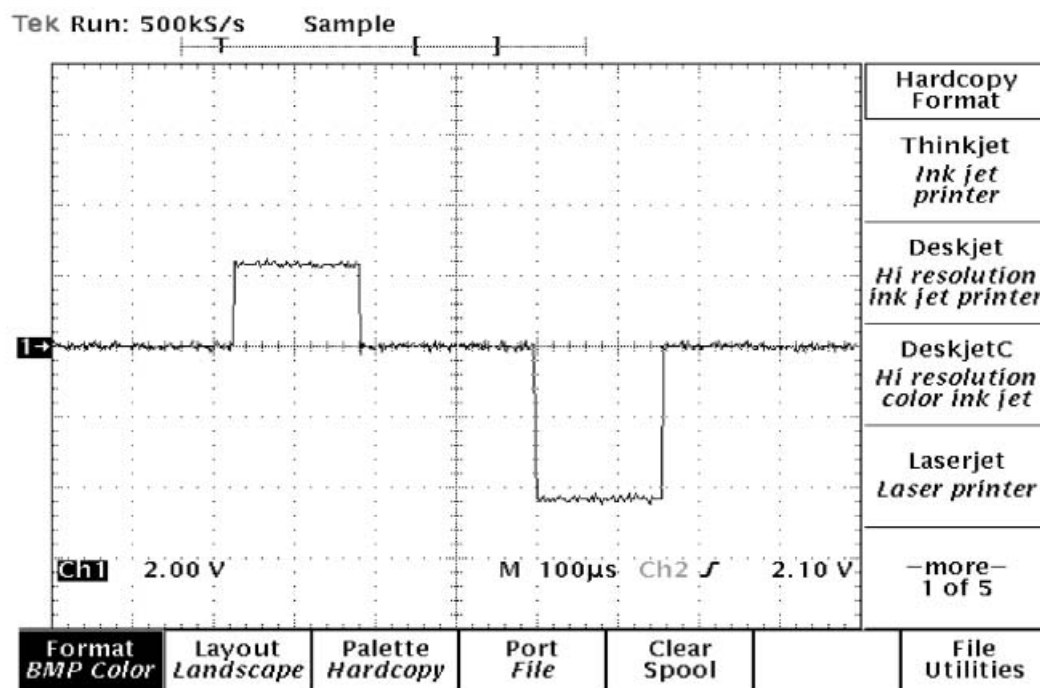


FIG. 7. Independent amplitude variability of the anodic phase.

and power goals would not be met. Several modifications are required in circuit design to meet the requirements. The digital circuit for the new IC will be more complex. Scaling to a smaller feature size technology directly results in digital circuit reduction. It was noticed that the same order of reduction in the area would not be possible for analog circuits, as the current output level remained the same. The next generation IC will be designed using TSMC 0.35  $\mu\text{m}$  process technology in place of the present AMI 1.2  $\mu\text{m}$  process and hence an area reduction up to nine times can be achieved due to a three times smaller feature size. A further improvement is from the fact that TSMC 0.35  $\mu\text{m}$  has four metal layers compared to two metal layers in AMI 1.2  $\mu\text{m}$  and hence has higher circuit density. A 1 : 8 output demultiplexing is used because each driver can stimulate eight pixels, as each pixel is active only for 2 ms in a period of 16.67 ms (at 60 frames per second). As anodic and cathodic pulses are not applied at the same time, a single DAC is used. A single DAC not only reduces the area but also reduces any current amplitude mismatch between anodic and cathodic pulses. Reducing the headroom required by the current mirror can significantly decrease the power dissipated in the output driver stage. Using active feedback current mirrors, we can make the output stage operate with lower headroom and still achieve higher output impedance for the current mirror. The maximum voltage drop across the output device can reach up to 12.5 V. Because the TSMC 0.35  $\mu\text{m}$  thick oxide devices are fabricated for 5 V, a higher voltage between the gate and drain can lead to gate oxide breakdown. This can usually be overcome by using high voltage transistors at the output stage. However, there are three drawbacks in using a high voltage transistor: (i) matching of the low voltage and high voltage transistors; (ii) the large size of a high voltage device; and (iii) the large series resistance at the drain region. So the use of high voltage transistors is to be avoided if possible. The solution lies in using low voltage transistors and dynamically biasing the devices to avoid a higher voltage appearing across its terminals.

The aim is to achieve a system lifetime of more than a decade, as implantation is a one-time process. So the reliability of the devices must be considered during the circuit design. The operating condition of the devices ought to be such that they can function reliably for 20–30 years. We have used MOSIS data to study the reliability and make sure that the design would not violate the reliability requirement. Also, matching of transistors in critical blocks such as current mirrors across 1,000 electrode outputs is to be

ensured in order to achieve charge-balanced anodic and cathodic outputs.

### Packaging

The package of the entire system should provide a hermetic seal to the chip to avoid malfunctioning due to the biological fluid surrounding the eye and also to provide electrical isolation for the tissue around the chip. The hermetic package should not only encapsulate the electronics but should also provide connections. Polymers such as silicon and fluoropolymers have been successful in accelerated life testing. Silicon, stainless steel, and titanium are generally used to encapsulate implants. Currently related work is in progress at one of our research partner institutions.

### Intraocular electromagnetic and thermal radiation

The implant will change the steady state temperature in the eye. There are two main reasons for this change. First, heat is generated due to the absorption of electromagnetic radiation in tissues. This electromagnetic radiation is generated by the power and data radio frequency link. Second, heat is generated by the implanted chip. Simulations were performed in order to verify that the level of radiation and temperature increase were within the safety limits. While 3-D modeling is an effective way to predict these changes, only a 2-D human eye model could be simulated due to the modeling complexities involved. The head model from the *visible human* project (22) was used. A fine grid of 0.25 mm was used to discretize the model. To verify the model accuracy, simulations were performed on analytically verifiable structures and were found to be accurate. It was noticed that, these simulations required not only developing and solving mathematical equations but also the use lot of data regarding tissue properties. For this reason, the results were compared with medically observed data.

The numerical FDTD (finite difference time domain) method was used for the radiation simulations (7). The specific absorption rate (SAR) of tissue was calculated by positioning the coil in front of the left eye. SAR is a measure of the power absorbed per unit of mass in a tissue due to exposure to electromagnetic waves. SAR is a function of the frequency of operation and simulations were performed at various frequencies (primarily at 2 MHz). The simulation requires solving the Maxwell equations. Equations are modified to 2-D and are discretized in time and space. To avoid reflecting waves from the boundary, a perfectly matched layer (PML) is used.

PMLs have exponentially increasing conductivity with respect to the penetration depth, so that all the wave energy is absorbed. Finally, Bio-heat equations were developed to calculate the temperature increase due to SAR and chip-generated heat. Because blood flow at the back of the retina conducts a lot of heat, it results in a lower temperature increase. The blood is modeled to have a constant temperature of 37°C. The increment time step was chosen such that it results in a reasonable simulation time. The given arrangement results in a maximum SAR of 404 mW/kg over the right eye for a coil placed over the left eye and operating at a frequency of 2 MHz (7,23). This results in a maximum temperature rise of 0.0685°C and if the choroidal blood flow rate is considered, it results in a maximum temperature rise of 0.0479°C at 37°C. The largest temperature increase is due to the power dissipated by the simulator IC. The maximum power dissipation is 46 mW for the 60 output Retina-3.55 chip. Worst case temperature increases, with and without choroidal blood flow, are 0.6123°C and 0.4349°C, respectively. It should be pointed out that the worst case temperature increase on the retina is 0.1876°C.

## RESULTS

### Telemetry unit

Through H-spice simulations the telemetry unit has been verified. Unlike typical implementations of forward/reverse telemetry links, the reverse telemetry link can be continuously operational because the forward data telemetry is operated at a much higher

frequency. The voltage regulator provides stable power supply rails of 7/14 V isolating the supply not only from the energy bursts in the power carrier due to reverse telemetry, but also from the internal current consumption variations and sharp on/off loading transitions (i.e. standby-mode to fully functional). Simulation results show that the non-dropout mode voltage regulation results in a worst-case peak power supply variation of 219 mV, for a regulation efficiency of approximately 1.5%. Measurements show satisfactory results at the design data rate of 25–250 kbps. It was found that the ASK and PWM demodulator circuits could be operated in excess of 1 Mbps, if the modulation index was increased to 30%. This rate is sufficient to operate the 1,000 output chip implant. It was also found that the interdependency of the data rate and carrier could be removed at a frequency ratio above 40.

### Stimulus chip

The Retina-3.55 stimulator IC was implemented using AMI 1.2  $\mu\text{m}$  technology. The chip shown in Fig. 8 has an area of  $4.6 \times 4.7 \text{ mm}^2$ . A typical biphasic stimulus output generated across a load of 10 k $\Omega$  is shown in Fig. 6. This is a transient plot of the voltage across the load resistance. The output is characterized in terms of functionality, linearity, anodic/cathodic matching, and variation across the chip.

## CONCLUSION

While circuit level details and results should have been discussed in more detail, only a summary of our efforts is presented here due to limited space. It should be noted that although the stimulus circuit and telemetry work presented here are designed for retinal prosthesis, the research would also benefit other implants. It should also be mentioned here that projects of this nature require expertise in many fields, such as biomedicine, chemistry, electronics and material science, and inputs from these other fields will be incorporated in the future designs.

## REFERENCES

1. Humayun M, de Juan E Jr, Weiland JD, Dagnelie G, Katona S. Pattern electrical stimulation of the human retina. *Vision Res* 1999;39:2569–76.
2. Liu W, McGucken E, Cavin R, Clements M, Vichienchom K, DeMarco C, Humayun M, de Juan E, Weiland J, Greenberg R. A retinal prosthesis to benefit the visually impaired. In: Horia-Nicolai L, Teodorescu N, Lakshmi CJ, eds. *Intelligent Systems and Technologies in Rehabilitation Engineering*. CRC Press, 2000;31–92.
3. Wyatt J, Rizzio J. Ocular implants for the blind. *IEEE Spectrum* 1996;00:47–53.
4. Chow AY, Chow VY. Subretinal electrical stimulation of the rabbit retina. *Neuroscience Letters* 1997;225.

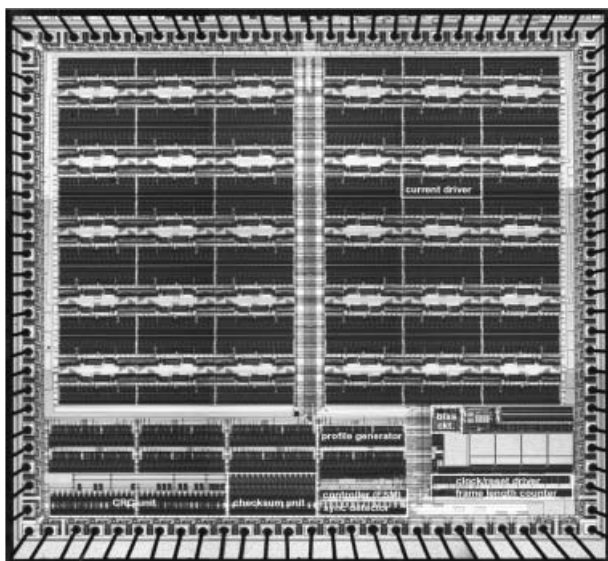


FIG. 8. Retina-3.55 photograph (4.6 mm  $\times$  4.7 mm).

5. Zrenner E, Stett A, Weiss S, Aramant RB, Guenther E, Kohler K, Miliczek KD, Seiler MJ, Hammerle H. Can sub-retinal microphotodiodes successfully replace degenerated photoreceptors? *Vision Res* 1999;39:2555–67.
6. Humayun M, de Juan E Jr, Weiland J, Dagnelie G, Katona S, Greenberg R, Suzuki S. Pattern electrical stimulation of the human retina. *Vision Res* 1999;39:2569–76.
7. DeMarco S. The architecture, design, and electromagnetic and thermal modeling of a retinal prosthesis to benefit the visually impaired. PhD Dissertation. Raleigh, NC: North Carolina State University. December 2001.
8. Rucker L, Lossinsky A. Percutaneous connectors. *30th Neural Prosthesis Workshop*, NINDS, NINCD, NIH, 12–14 October 1999.
9. Zierhofer C, Hochmair E. High-efficiency coupling-insensitive transcutaneous power and data transmission via an inductive lin. *IEEE Trans Biomed Eng* 1990;37:716–22.
10. Zierhofer C. A class-E tuned power oscillator for inductive transmission of digital data and power. *Proceedings of the 6th Mediterranean Electrotechnical Conference* 1991;1:789–92.
11. Zierhofer C, Hochmair E. Geometric approach for coupling enhancement of magnetically coupled coils. *IEEE Trans Biomed Eng* 1996;43:708–14.
12. Kadefors R, Kaiser E, Petersen I. Energizing implantable transmitters by means of coupled inductance coils. *IEEE Trans Biomed Eng* 1969;BME-16:177–83.
13. Donaldson P. Power for neurological prostheses: a simple inductive RF link with improved performance. *J Biomed Eng* 1987;9:194–7.
14. Von Arx J, Najafi K. A wireless single-chip telemetry powered neural stimulation system. *IEEE International Solid State Circuits Conference*, 1999;214.
15. Nardin M, Najafi N. A multichannel neuromuscular microstimulator with bi-directional telemetry. *8th International Conference on Solid State Sensors and Actuators*, Eurosensors IX, 1995;59–62.
16. Sokal N, Sokal AD. A class-E: a new class of high-efficiency tuned single-ended switching power amplifier. *IEEE Journal of Solid State Circuits* 1975;SC-10:168–76.
17. Sokal N. Class-E: high-efficiency switching-mode tuned power amplifier with only one inductor and one capacitor in load network—approximate analysis. *IEEE Journal of Solid State Circuits* 1981;SC-16:381–4.
18. Bashirullah R, Liu W, Kendir G, Ji Y, Sivaprakasam M, Wang G, Pundi S. A smart bi-directional telemetry unit for retinal prosthetic device. *ISCAS* 2003;5:5–8.
19. Majji A, Humayun M, Weiland J, Suzuki S, D'Anna S, de Juan E Jr. Long-term histological and electrophysiological results of an inactive epi-retinal electrode array implantation in dogs. *Invest Ophthalmol Vis Sci* 1999;40:2073–81.
20. Liu W, Vichienchom K, Clements M, DeMarco S, Hughes C, McGucken E, Humayun M, Weiland J, Greenberg R. An arbitrary waveform stimulus circuit for visual prostheses using a low area multibias DAC. *IEEE Journal of Solid State Circuits* 2000;35:1487–97.
21. Dagnelie G, Barnett D. Simulations of Prosthetic Vision. Available at: <http://www.irp.jhu.edu/media/index.htm>.
22. The National Library of Medicine. The Visible Human Project. Available at: <http://www.nlm.nih.gov/research/visible/visiblehuman.html>.
23. Lazzi G, DeMarco S, Liu W, Humayun M, Weiland J. Simulated temperature increase in a head/eye model containing an intraocular retinal prosthesis. *2001 IEEE International Symposium Antennas and Propagation Society* 2001;2: 72–5.